Comparative study by numerical simulation of two methods for automatic flow control in centrifugal pumps

Rogger José Andrade-Cedeno[1,2], Jesús Alberto Pérez-Rodríguez[3], Carlos David Amaya-Jaramillo[4], Ciaddy Gina Rodríguez-Borges[5], Endrickson Ramón Vera-Cedeno[2], Luis Santiago Quiroz-Fernández[6], Yolanda Eugenia Llosas-Albuerne[3]

[1]Investigador asociado al Posgrado en Instrumentación, Facultad de Ciencias, Universidad Central de Venezuela (UCV), Caracas, Venezuela
[2]Unidad Académica de Formación Técnica y Tecnológica, Universidad Laica Eloy Alfaro de Manabí (ULEAM), Tosagua, Ecuador
[3]Departamento de Electricidad, Facultad de Ciencias Matemáticas, Físicas y Químicas, Universidad Técnica de Manabí (UTM), Portoviejo, Ecuador
[4]Departamento de Electricidad, Facultad de Ciencias de la Ingeniería. Universidad Técnica Estatal de Quevedo (UTEQ), Quevedo, Ecuador
[5]Departamento de Ingeniería Industrial, Facultad de Ciencias Matemáticas, Físicas y Químicas, Universidad Técnica de Manabí (UTM). Portoviejo, Ecuador
[6]Departamento de Ingeniería Civil, Facultad de Ciencias Matemáticas, Físicas y Químicas, Universidad Técnica de Manabí (UTM), Portoviejo, Ecuador

Article Info

ABSTRACT

Flow rate and pressure are variables of great interest in the process control industry, especially in pumping systems. With the help of modeling and simulation, it is possible to understand the operation of these systems prior to their construction, in addition to allowing their behavior to be analyzed in various operational scenarios and testing different control strategies. In this work, the hydraulic, mechanical, electrical and electronic models of the different components of the system are studied. Two study cases for automatic flow control are assembled, using Simscape library from MATLAB/Simulink R2019b. This study cases are: i) with a control valve and ii) with a variable speed drive. The simulations determined that both cases keep the flow constant in the face of pressure disturbances, with a good dynamic response. Case 2 consumes less power than case 1, between 24 and 64% less, especially at low flow rates. It also reduce unwanted mechanical and electrical problems due to sudden starts and stops. Case 2 produced harmonic pollution on both the grid and motor sides, which implies a potential risk for the motor and the electrical grid. Case 2 was experimentally validated, obtaining errors of less than 10%.

Corresponding Author:

Rogger José Andrade-Cedeno
Investigador asociado al Posgrado en Instrumentación, Facultad de Ciencias, Universidad Central de Venezuela (UCV)
Caracas 1040, Distrito Capital, Venezuela
Email: rogger.andrade@gmail.com

1. INTRODUCTION

Pressure and flow control systems are widely used in the pumping, transportation, distribution and handling of fluids. They are found in crude oil transportation systems [1], in aqueducts for pumping and water distribution [2], and in pressurized irrigation systems [3], among others. It is common in these systems to find centrifugal pumps, induction motors, variable frequency drives, control valves, electronic

instrumentation and controllers, since the combination of several of them allows the implementation of an automatic pressure or flow control system according to the needs of each application, and a laboratory experimental application can be seen in [4]. In the case of pumping systems, there are two methods to regulate the capacity: i) by throttling with a control valve and ii) by varying the speed of the electric pump with a variable speed drive, the second method being the most efficient [5]. However, this does not mean that the control valve has lagged behind; on the contrary, it is still considered the most used final control element in the process control industry [6]. Gevorkov *et al.* [7] consider that throttling control is still widely used in industry, and simulated an electric actuator coupled to a control valve for a pumping application, the results of which determined that the pressure could be regulated by precise position control achieved by the electric actuator. In the same way, Vijayalakshmi *et al.* [8], they simulated and implemented a closed loop flow control using a control valve with proportional integral derivative (PID) algorithm. On the other hand, Andrade-Cedeno and Perez-Rodriguez [9] simulated a pulse-width modulation voltage-source inverter (VSI-PWM) type variable speed drive, governed by a scalar control strategy with a constant V/f ratio combined with the space vector modulation (SVM) technique. The analysis determined that this technology performs well for applications with induction motors coupled to centrifugal machines such as pumps, compressors and fans. Several investigations on automatic control in pumping systems have been developed. Shankar, et al. [10] simulated two centrifugal pumps in parallel at variable speed and studied the pressure and flow response for various speeds. Furthermore, they determined that a 50% reduction in speed produces an 80% reduction in power. Gevorkov *et al.* [11] simulated a constant pressure system on a variable speed centrifugal pump, adding a pressure sensor for feedback and an automatic proportional integral (PI) controller. The simulated model was experimentally validated, finding differences in steady state from 7 to 14%. Gevorkov *et al.* [12] carried out a mixed simulation and experimentation study of a flow control system with a variable speed centrifugal pump, using a flow sensor for feedback and a PI controller. The inaccuracy of the proposed model varied between 0.3 and 4%. In the research by Wu *et al.* [13], they compared the use of a variable speed drive (speed regulation) versus the use of a control valve (discharge throttling), and it was determined that the speed control method requires 37% less power than the discharge throttling method.

This research describes the models of the typical components of a water pumping and distribution system, made up of: the piping system, centrifugal pump, induction motor, variable speed drive, control valve, and control system. Using Simscape library from MATLAB/Simulink R2019b, two case studies are simulated to achieve automatic flow control: i) with a control valve and ii) with variable speed drive. The dynamic response of the system, the starting current, the harmonic distortion and the power saving are analyzed.

2. METHOD
2.1. Capacity regulation in centrifugal pumps
Figure 1 shows the characteristic curves of a centrifugal pump with the operating points for different capacity control methods. In nominal conditions, the pump must operate at the best efficiency point (BEP), which is very suitable in systems with fixed demand that are well designed and dimensioned. If the demand changes, the system curve also changes and it operates at a different point of the BEP.
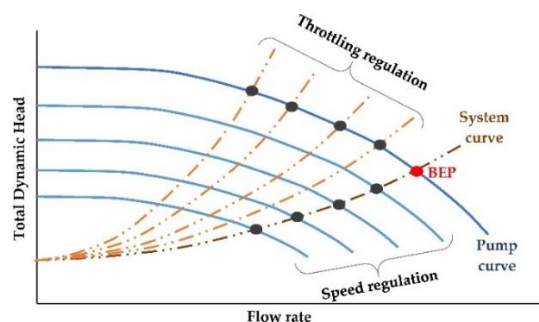

Figure 1. Methods for capacity regulation in centrifugal pumps

Operating a centrifugal pump too far from the BEP, either to the right or to the left of the curve, can put the equipment at risk from adverse effects such as cavitation, vibration, impeller damage, suction or discharge recirculation, and reduced life of seals and bearings [14]. To prevent these problems, the

centrifugal pump must be operated in the preferred operating region (POR), which is between 70 and 120% of BEP [15]. When regulating the output of the pump with a control valve, the valve changes the dynamic head of the system, causing the system curve to intersect with the pump curve at the new operating point. While on the one hand the throttling reduces the flow rate, on the other hand the pump is forced to produce a higher dynamic head (higher pressure). When using variable speed control the system curve remains unchanged, while the pump curve moves down according to the speed change, and the operating point moves to a new intersection between the two curves. The benefit of controlling the speed of the pump is that the efficiency drops much less compared to the use of a control valve [16].

2.2. Study cases

Figure 2 shows the two study cases to be simulated. Case 1 is shown in Figure 2(a), where a control valve with an electric actuator is used on the pump discharge for automatic flow control. Case 2 can be seen in Figure 2(b), and in this case a variable frequency drive coupled to the electric motor is used. The models are obtained from the Simscape library of Simulink, in version R2019b of MATLAB. These tools are specialized in the modeling and simulation of physical, mechanical, hydraulic, electrical, electromechanical, mechatronic, and automatic control systems.
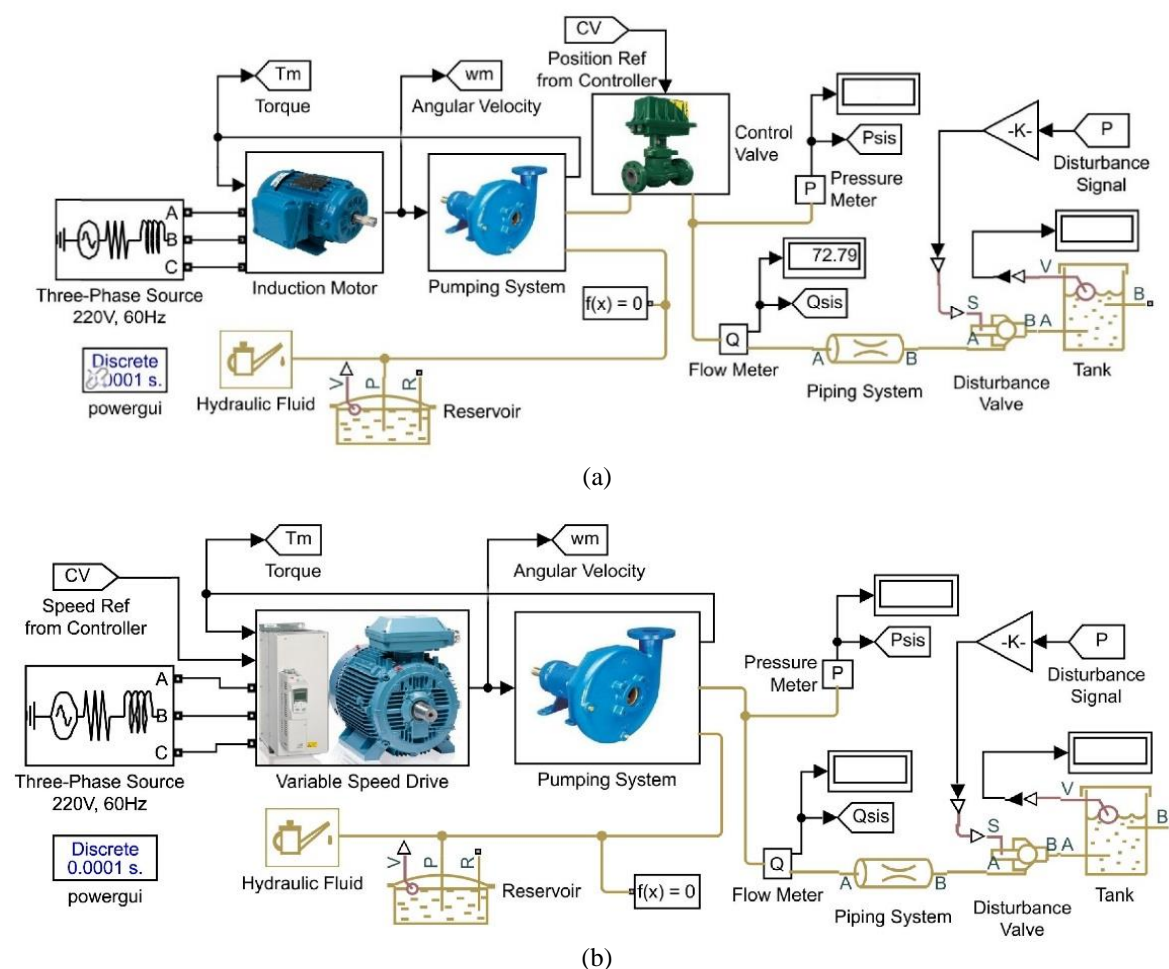

(a)

(b)

Figure 2. Study cases for (a) flow control system based on control valve with electric actuator and (b) flow control system based on variable speed drive on the pump

2.3. Piping system

For the pipe system model, the pressure loss due to friction is calculated using the Darcy equation. The friction factor in the turbulent regime is determined with the Haaland approximation. The friction factor during the transition from laminar to turbulent regimes is determined by linear interpolation between the extreme points of the two regimes [17].

2.4. Pumping system

Figure 3 shows the model of the pumping system, made up of the centrifugal pump as the main component. For centrifugal pump characterization, the performance curves provided by the manufacturer are used to form two one-dimensional search tables: i) differential pressure vs flow rate and ii) brake power vs flow rate. Both characteristics are specified at the same reference angular velocity, and at the same fluid density. To obtain the differential pressure at another angular velocity, the laws of affinity are used [18].
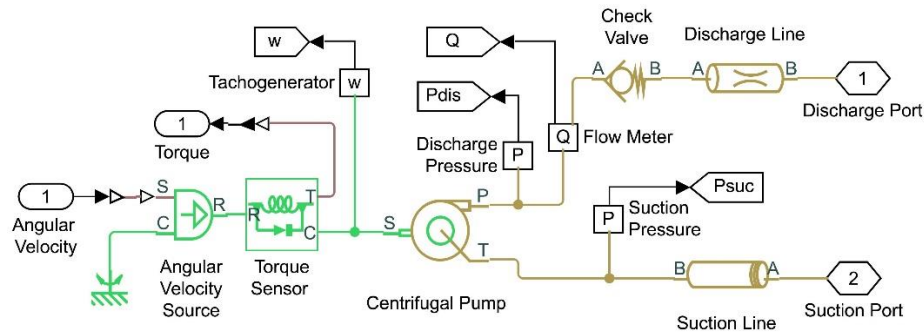

Figure 3. Pumping system model

2.5. Control valve with electric actuator

Figure 4 shows the integrated model of the control valve with electric actuator. The control valve is modeled using the flow coefficient provided by the manufacturer [19]. The driving source of the actuator is a DC motor [20]. The mechanical output of the DC motor enters the ideal, non-planetary, fixed gear ratio gearbox [21]. The gear ratio is determined as the ratio of the angular velocity of the input shaft to that of the output shaft. The gearbox output connects to the rack and pinion block, which converts rotational to translational motion [22]. The DC motor drive has a control component and a power component. The control component consists of a pulse-width modulation (PWM) system, which receives the signal from the main control system to adjust the trigger signals to the power component. The power component consists of power semiconductors (usually BJTs, MOSFETs, or IGBTs) in an H-bridge connection scheme.
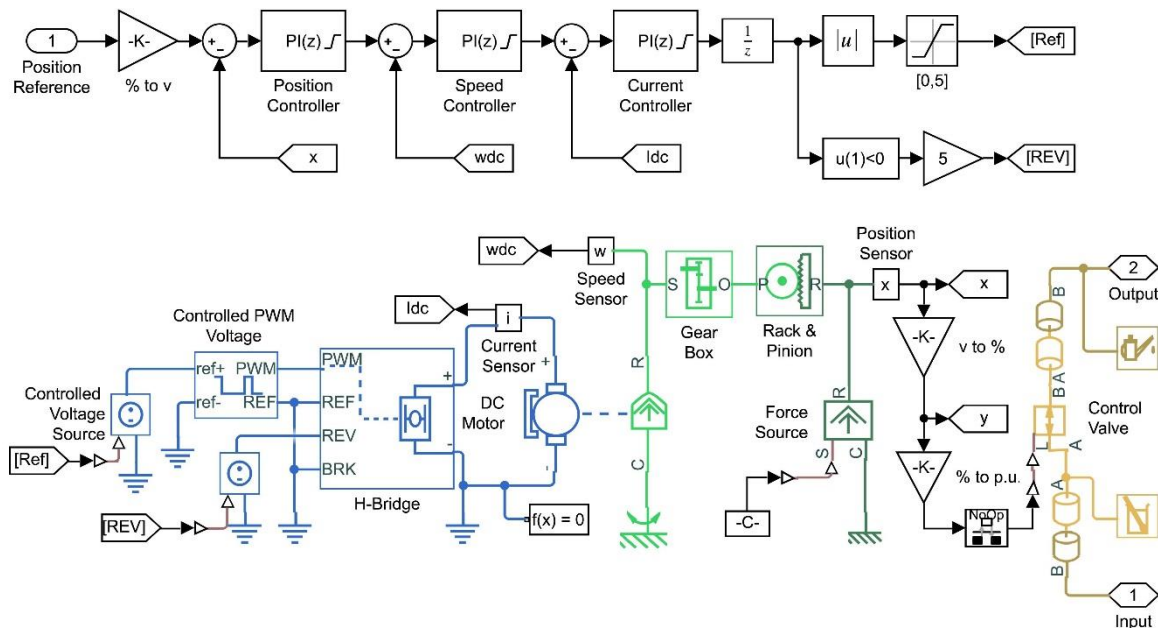

Figure 4. Model of control valve with electric actuator

The PWM system modulates the switching of the power semiconductors, thus controlling the polarity and amplitude of the voltage fed to the DC motor, and therefore its speed and rotational direction [23]. The main control system for the linear electric actuator consists of a three-loop cascade control. The innermost loop is a PI controller of the motor current, whose feedback signal is achieved by a current sensor, and directly modifies the PWM signal going into the H-bridge. The middle loop consists of a PI controller of the motor speed, which is fed back from a speed sensor. The outermost loop is for linear position control of the system, and receives feedback from a linear position sensor. For fast response and safe operation, each control system loop must be precisely designed [24], [25].

2.6. Induction motor

The induction motor is based on the asynchronous machine model. The stator and rotor windings are Y-connected with internal neutral. A sixth-order state space model for the double-cage machine and a fourth-order state space model for the single-cage machine represent the electrical component. The mechanical component is modeled as a second order system. All electrical variables and parameters are referred to the stator; furthermore, the stator and rotor quantities are in an arbitrary two-axis frame of reference [26]. The two-axis reference frame, known as the dq reference frame, is the result of applying the Clarke and Park transforms [27]. The induction motor is used in two schemes: with direct connection to the grid (frequency and nominal speed, Figure 5(a)), and as a part of a variable speed drive (frequency and variable speed, Figure 5(b)).
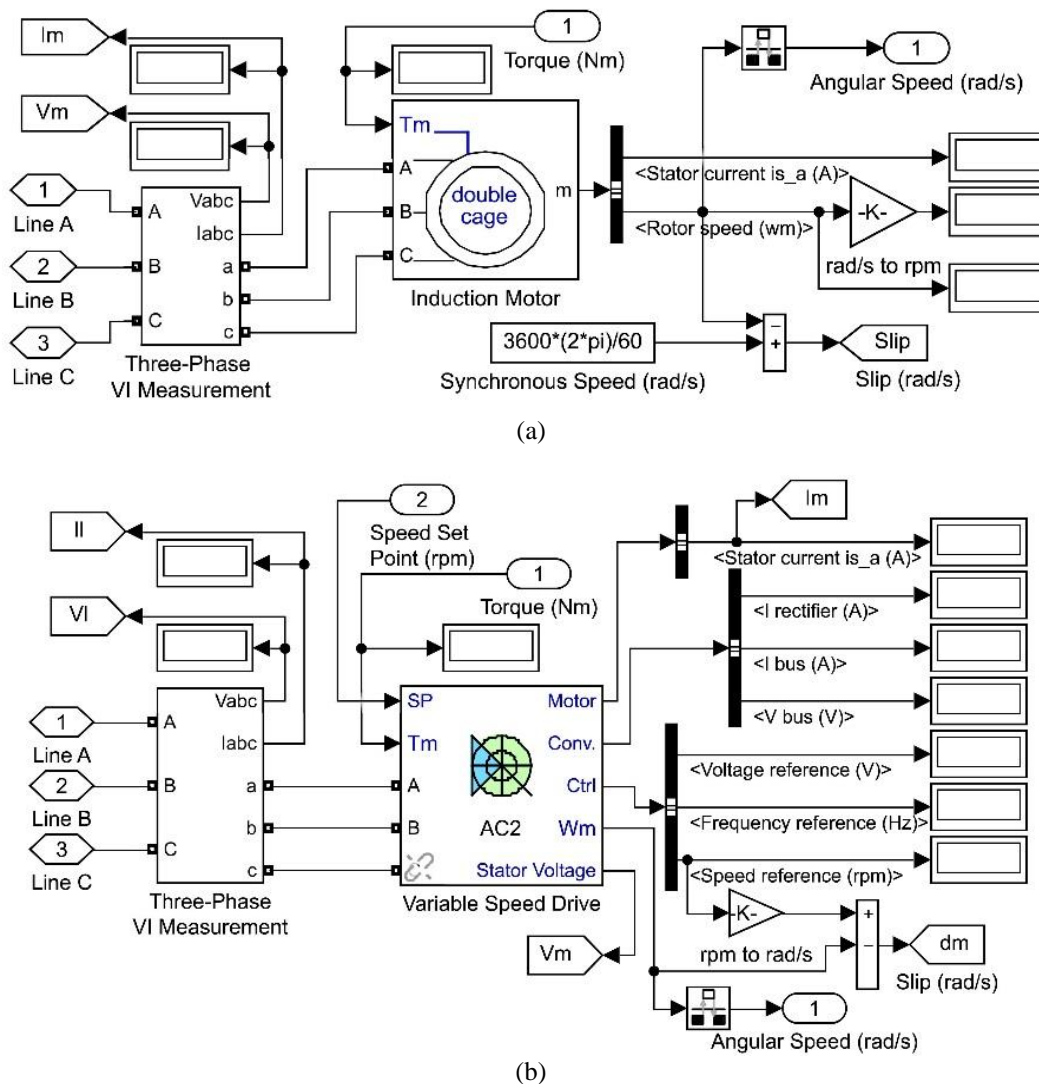

(a)

(b)

Figure 5. Three-phase induction motor models with their drives and meters for (a) direct connection to the grid and (b) variable speed drive system

2.7. Variable speed drive

The variable speed drive model is based on the block drive AC2 "Space vector PWM VSI induction motor drive", which contains an asynchronous machine controlled by a variable frequency drive [28]. The asynchronous machine is configured as a three-phase induction motor, and its variable frequency drive contains the following components: the three-phase rectifier formed by diodes; the DC link formed by a capacitor; the three-phase inverter formed by IGBTs; and the control system formed by a speed controller and a space vector modulator (SVM) [29], as shown in Figure 6(a).

The control system has a closed-loop speed control, made up of the classic V/f scalar control plus a slip compensator based on a PI algorithm [30], as seen in Figure 6(b). The speed control loop receives the speed reference (N^*) and subtracts it from the current speed (N) measured with the speed sensor, to obtain the motor slip (speed error). Then, the PI algorithm computes and compensates for the slip in the current speed (N). The PI compensator parameters, K_p and K_i, were tuned using the Ziegler-Nichols method.
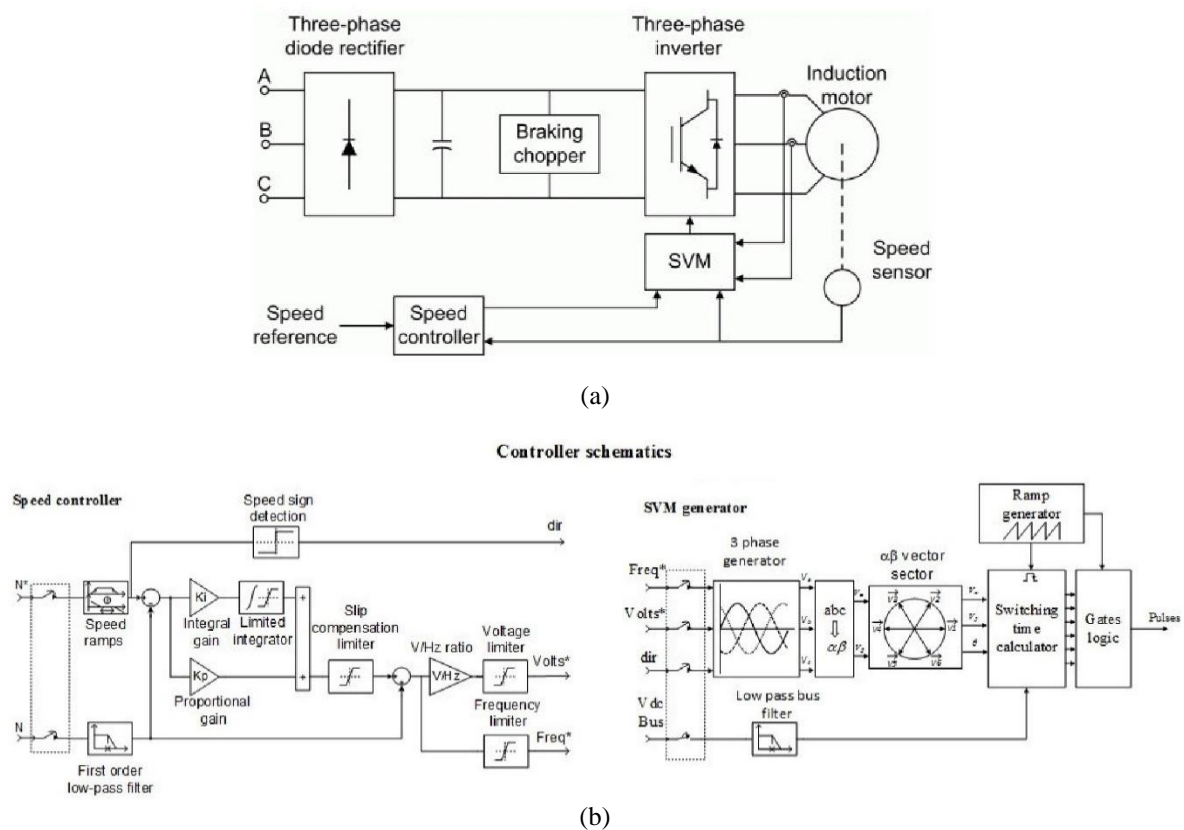

(a)

(b)

Figure 6. AC2 drive model block diagrams for (a) general block diagram and (b) block diagram of control system

The frequency reference ($Freq^*$), and the voltage reference ($Volts^*$), are obtained from the constant V/f ratio block, and are used as inputs to the space vector modulator (SVM) stage, as seen in Figure 6(b). The SVM technique starts with a three-phase signal generator, whose signals are then converted to the αβ reference frame using the Clark transform block. This is necessary to run the SVM algorithm, which produces the controlling signals of IGBTs. SVM has better performance than other PWM techniques because of better utilization of the DC bus and least harmonic distortion production [31].

2.8. Automatic control system

Figure 7 shows the block diagram of the automatic flow control system, when a control valve with an electric actuator is used (Figure 7(a)), and when a variable speed drive is used (Figure 7(b)). In both cases, the main control loop is executed with the PI flow controller, which commands the controls embedded in the electric actuator or in the variable speed drive (described above). Feedback is achieved with a flow transmitter (flowmeter).
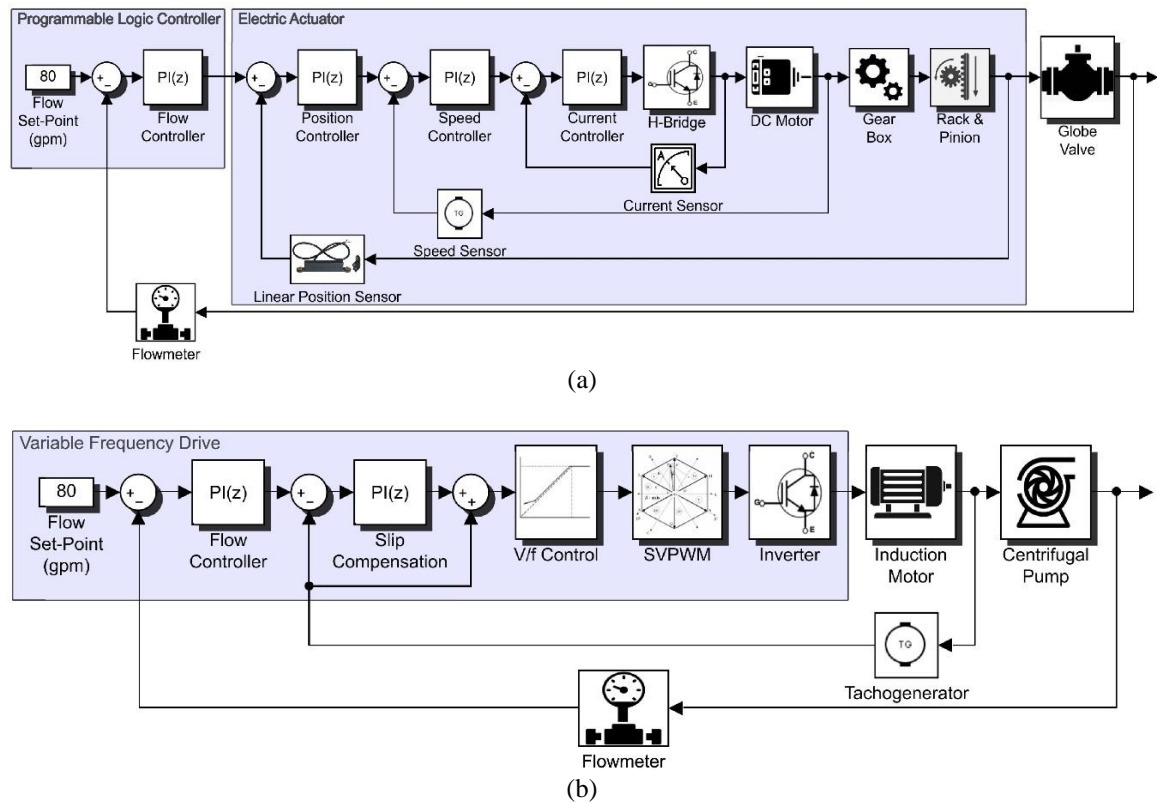
(a)

(b)

Figure 7. Block diagram of the automatic flow control system for (a) based on control valve and electric actuator and (b) based on variable speed drive

3.   RESULTS AND DISCUSSION

For simulation, a 110 gpm @ 32 m centrifugal pump was used, with a 5 hp, 3 ph, 220 V, 60 Hz, 3450 rpm induction motor, in addition to a globe type control valve, equal percentage, 2 inches and Cv of 33.2.

3.1. Dynamic response of the control system

Figure 8 shows the dynamic response of several variables of interest, for the two cases studied. Both cases met the objective of maintaining constant flow at a set point of 70 gpm, in the face of pressure disturbances produced by the disturbance valve. The control system specifications, such as the response time, overshoot and position error, will depend on the requirements and characteristics of each process to be controlled.

In case 1 (Figure 8(a)), with the pump at nominal speed and the control valve in discharge, the mechanical and hydraulic variables of the pump remained more or less constant during the steady state, with transients produced by pressure changes. The pressure drop across the control valve resulted from the difference between the pump discharge pressure and the system pressure, and increased when the control valve had a lower position. This pressure drop represents energy losses for the system [13]. Also observed was the dynamic response of the three variables from the cascade control of the actuator: current (internal loop), speed (medium loop), and position (external loop). The response time was lower the more internal the control loop was, which is required for the adequate performance of the cascade control [24].

In case 2 (Figure 8(b)), there was no restrictive element in the pump discharge, and the speed was automatically regulated to meet the flow requirement in the presence of pressure disturbances. The speed, the total dynamic head and the torque increased or decreased as the pressure disturbance did. This action allows power saving compared to case 1. In addition, the slip remained at zero thanks to the slip compensator part of the control system of the variable speed drive. This helps improve the operating performance of the induction motor [32].
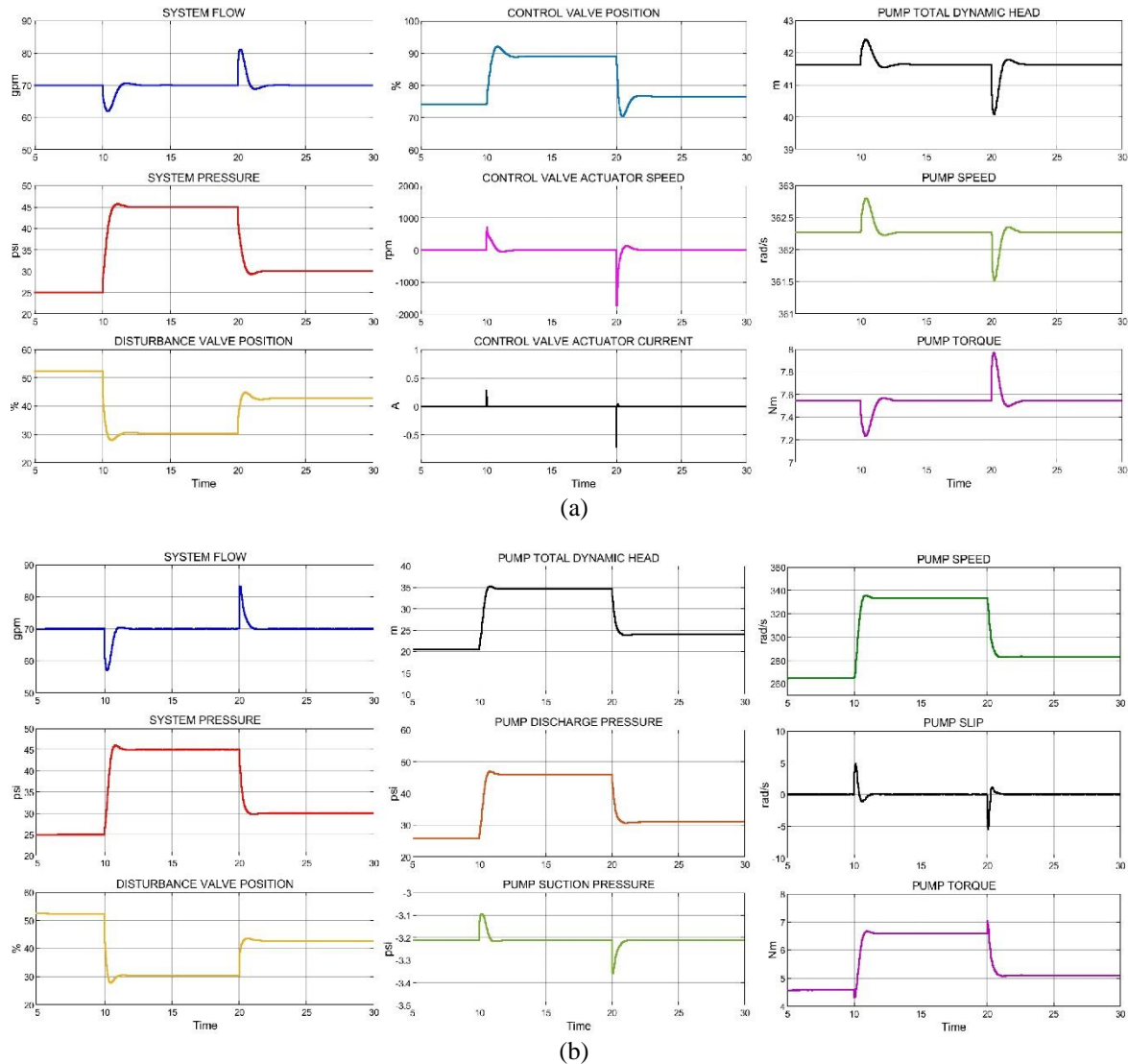
Figure 8. Dynamic response of several variables of interest for (a) case 1: fixed speed pump with control valve with electric actuator and (b) case 2: variable speed pump with the use of variable speed drive

3.2. Operational efficiency, consumption and power savings

Table 1 shows a register of the various hydraulic and mechanical variables of interest. With the flow and pressure data the hydraulic power was calculated, with the torque and the angular speed the mechanical power in the shaft was obtained, and with these results the efficiency of the pump was calculated. In all scenarios, it was possible to meet the set point, but case 2 did so with greater variability. Reducing the set point reduced the efficiency of the pump, more significantly in case 1. With respect to mechanical power consumption, case 2 consumed less power than case 1, and this difference increased when reducing the set point. With this, a saving in mechanical power of case 2 was obtained with respect to case 1, from 24 to 64%.

In this analysis, the effect of the variable speed drive was not considered, given that under nominal conditions electric motors are more efficient than pumps, and variable speed drives more efficient than motors. However, the efficiency of the motor can change with variations in load torque and speed [33]-[35]. Burt *et al*. [35] analyzed that the efficiency of the electrical system with variable speed drive can be reduced by up to 8% compared to the system with direct connection to the grid. However, the study concluded that this reduction is not significant in relation to the energy savings achieved with a variable speed drive, since the drive adjusts the speed of the process to the changing demand conditions.

Table 1. Operational data recording

Set point	Flow rate		Pressure		Angular speed		Torque		Pump efficiency		Shaft power		Power saving
	Case 1	Case 2	Case 1	Case 2	Case 1	Case 2	Case 1	Case 2	Case 1	Case 2	Case 1	Case 2	
gpm	gpm	gpm	psi	psi	rpm	rpm	Nm	Nm	%	%	kW	kW	%
100	100	100.00	35	35.01	3440	3080	8.67	7.33	73.81	74.55	3.12	2.36	24.34
100	100	100.00	30	30.01	3440	2924	8.67	6.78	73.81	74.41	3.12	2.08	33.55
100	100	100.10	25	25.00	3440	2758	8.67	6.21	73.81	74.03	3.12	1.79	42.58
70	70	70.00	35	34.99	3459	2875	7.54	5.61	65.90	70.67	2.73	1.69	38.22
70	70	70.01	30	30.00	3459	2707	7.54	5.10	65.90	72.00	2.73	1.45	47.08
70	70	69.99	25	25.00	3459	2528	7.54	4.58	65.90	73.24	2.73	1.21	55.62
40	40	40.07	35	35.03	3478	2742	6.40	4.25	46.66	55.03	2.33	1.22	47.66
40	40	39.93	30	29.96	3478	2562	6.40	3.78	46.66	57.19	2.33	1.01	56.43
40	40	40.11	25	25.04	3478	2376	6.40	3.34	46.66	59.87	2.33	0.83	64.35

3.3. Starting current and harmonic distortion

Figure 9 shows the waveforms of the currents and voltages of the induction motor during the starting process and in the stable state. Figure 9(a) shows the direct on-line starter (DOL) through direct connection to the grid (case 1), where the transient lasted approximately 250 ms (15 cycles). It is seen that the starting current was about 7.4 times the steady state current. On the other hand, Figure 9(b) shows the starting process through an acceleration ramp of 3600 rpm/s, provided by the variable speed drive (case 2). In this second case, the starting current did not exceed 2.8 times the steady-state current. When a pump operates at variable speed (case 2), the waveforms of the voltages and currents, on both the drive and the motor side, are as shown in Figure 9(c). The total harmonic distortion (THD) was obtained using the fast fourier transform (FFT), a tool of the specialized "powergui" block of Simulink. On the line side, a THDi of 82.69% and THDv of 4.31% were obtained, and on the motor side, a THDi of 20.55% and THDv of 48.42% were obtained. The variable speed drive (case 2) affects the quality of the energy on the motor and grid side.

3.4. Experimental results and model validation

Figure 10 shows case 2 experimental setup. The module is made up of a Gould 3656 centrifugal pump with a Baldor JMM3212T induction motor, electrical panels, control panel, and instrumentation. The control panel contains an ABB ACS310 variable frequency drive (VFD), and an XT sensor TUF-2000M ultrasonic flowmeter. The flow transducers, pressure transducer, and pressure gauge were installed in the discharge pipe. The flow transmitter and pressure transducer were connected with the analog inputs of the VFD, using 4-20 mA signals. The control algorithms (PI flow controller, PI slip compensator, V/f scalar control, and space vector modulation), were configured on the VFD. For data collection, a Dell Inspiron PC was used, with an Intel Core i7 processor and Windows 7 operating system, interconnected with the VFD and the Hantek 6022BL digital oscilloscope. The specifications of the centrifugal pump, at nominal conditions, are: capacity=110 GPM, total dynamic head=32 m, speed=3500 rpm, efficiency=75%. The selected three-phase induction motor has the following specifications at rated conditions: output power=5 hp (3.73 kW), voltage=208-230/460 V, current=13-12.2/6.1 A, speed=3450 rpm, frequency=60 Hz, power factor=89%, efficiency=85.5%. The ultrasonic flowmeter has the following specifications: accuracy=±1%, temperature=-30~160 °C, flowrate=0~±7 m/s, damping=10 s, output signal=4-20 mA, power supply=8 a 36 Vdc.

Figure 11(a) shows the pressure, flow, speed, and torque trend graphs during the experimental test, data obtained from the VFD using ABB's DriveWindow Light software. Since the software only graphs in percentages, all four variables were converted to percentages based on the range of the measurement. For the test, a set point of 50 GPM (46.67%) was set, and the manual valve in the pump discharge was manipulated to generate up and down pressure disturbances. As can be seen in Figure 11(a), the control system fulfills its objective of keeping the flow rate constant at the set point, in the face of pressure disturbances. In the transient state, the overshoot was less than 10% and the settling time was less than 20s, mainly influenced by the flowmeter time constant (10s) and PI flow controller parameters.

Figure 11(b) shows the pressure, flow, speed, and torque trend graphs resulting from the simulation, observing the similarity with the experimental results. Simulink models parameterization was done using equipment plate data and manufacturers' technical specifications. The parameterization of the centrifugal pump was carried out with the performance curves obtained from the catalog. In the case of the induction motor, the parameterization was done by entering the nameplate data into the optimizer provided by the asynchronous machine block in Simulink. For the simulated flowmeter, a transfer function of a first-order system with a time constant of 10 s was considered, to be consistent with the damping of the real-world flowmeter. Table 2 shows the relative error of the simulation concerning the experimentation for the steady-state condition, observing that, in none of the cases, the error exceeds 6%.
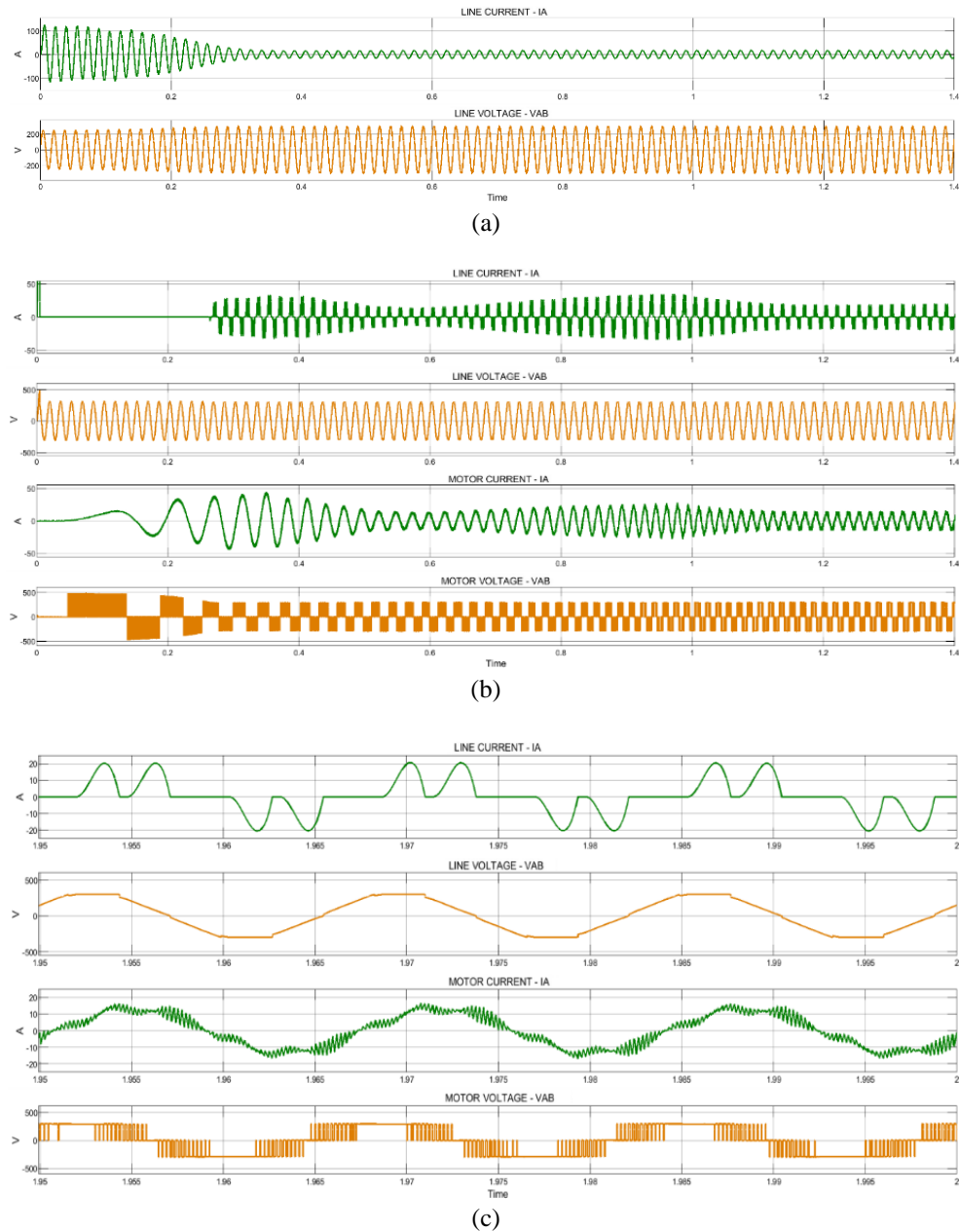
(a)

(b)

(c)

Figure 9. Currents and voltages at startup and steady state for (a) direct start, (b) soft start by means of the variable speed drive, at 3600 rpm/s, and (c) steady state signals when operating with variable speed drive

Figure 10. Experimental setup of flow control system with variable speed drive (case 2)
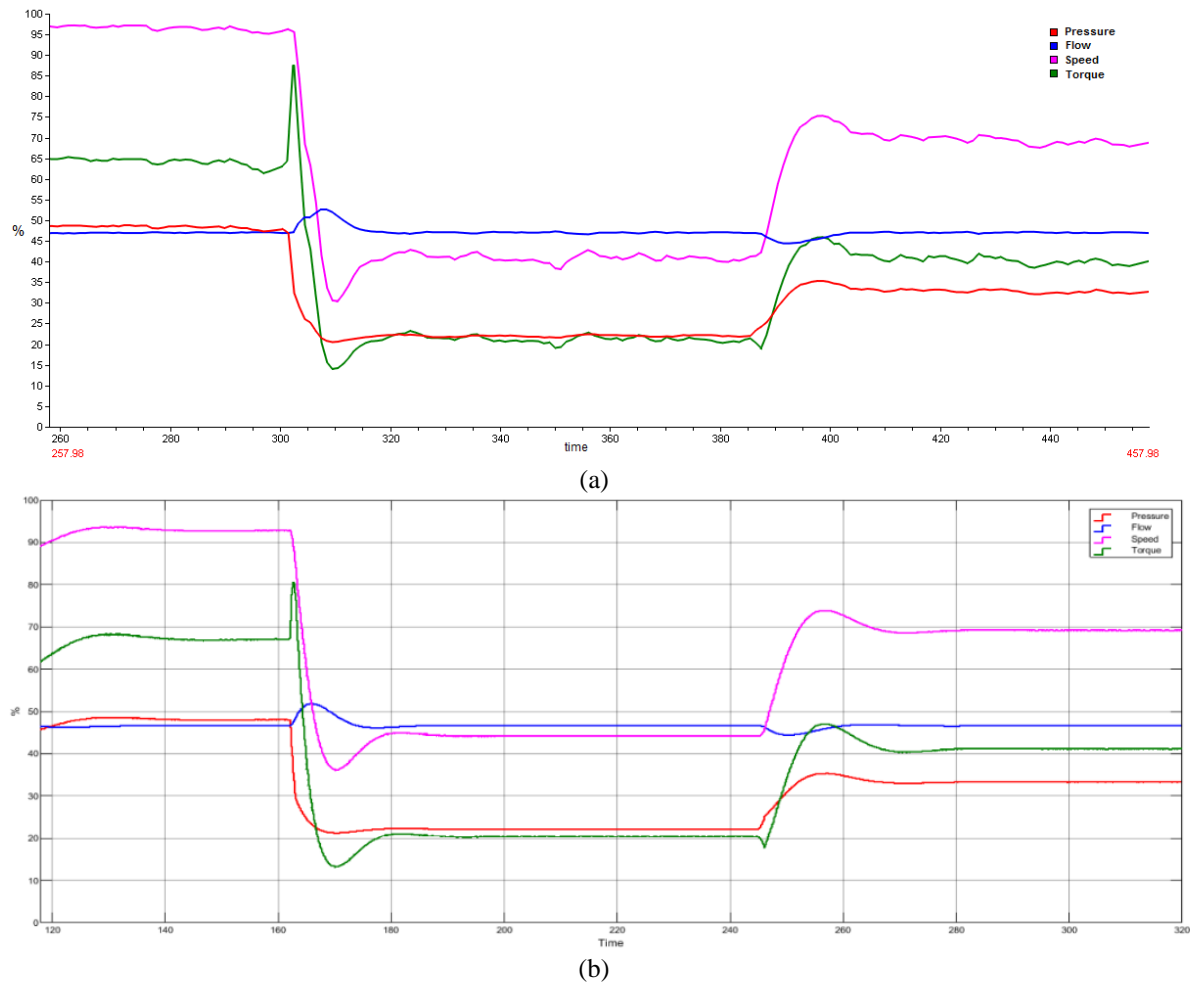
(a)

(b)

Figure 11. Model validation for (a) experimental results and (b) simulation results

Table 2. Hydraulic and mechanical variables validation

Simulation					Experimentation					Relative error				
Pressure %	Flow %	Speed %	Torque %	Freq. Hz	Pressure %	Flow %	Speed %	Torque %	Freq. Hz	Pressure %	Flow %	Speed %	Torque %	Freq. %
48.07	46.67	92.8	67	58.05	48.5	46.9	96.2	63.7	59.4	0.89	0.49	3.53	5.18	2.27
22.25	46.67	44.24	20.33	27.26	21.9	46.9	41.8	21.1	26.5	1.6	0.49	5.84	3.65	2.87
33.35	46.67	69.27	41.22	42.91	32.8	46.8	70.42	41	44.3	1.68	0.28	1.63	0.54	3.14

Figure 12 shows the electrical variables obtained with the oscilloscope during the experimental tests. What was predicted in the simulation concerning the starting current is corroborated, being more abrupt in the direct starting (Figure 12(a)), and softened when the acceleration ramp of 1s is configured in the VFD (Figure 12(b)). Therefore, the use of a variable speed drive limited the starting current by 62%, which is advantageous to prevent some hydraulic, mechanical, and electrical problems, such as water hammer and pressure surges [36], vibrations in the pipes [37], voltage drops in the motor and the electrical grid [38], and mechanical stress that reduces the useful life of the motor [39].

The line-side current has high harmonic distortion (Figure 12(c)), and a non-symmetrical waveform is observed, unlike what was obtained in the simulation. This asymmetry is due to the voltage unbalance in the power supply to the VFD [40]. The motor-side current is closer to the sine wave (Figure 12(d)), with the characteristic ripple produced by semiconductor switching. The line-side voltage has the lowest harmonic distortion among all the analyzed waves (Figure 12(e)), corroborating what was obtained in the simulation. The voltage transients on the motor-side, produced during the switching of the power semiconductors, are not observed in the simulation but are appreciated in the experimentation (Figure 12(f)). This leads to the phenomenon of the reflected wave, which is amplified if the distance between the VFD and the induction motor increases, generating damaging overvoltages for the conductors and the induction motor, and damaging overcurrents for the VFD [41], [42]. The motor-side voltage also has a high harmonic distortion as

a consecuence of the PWM control signal. Harmonics affect the power factor and efficiency of the induction motor and can also affect the behavior, reliability, and useful life of some of its mechanical components [43]. Harmonic pollution also affects the electrical grid and equipment connected to it, causing overload and overheating in transformers, as well as unwanted tripping of electrical protections, affecting lighting systems and causing interference in electronic equipment and communication systems [44]. Harmonics can be treated by implementing filters [45]. The validation of the electrical variables is shown in Table 3, where it is observed that the relative error of the simulation results does not exceed 10% concerning the real experimental data.

Figure 12. Oscilloscope waveforms for (a) direct start current, (b) soft start current (acceleration ramp set in 1 s), (c) line side current at 60 Hz, (d) motor side current at 60 Hz, (e) line side voltage at 60 Hz, and (f) motor side voltage at 60 Hz

Table 3. Electrical variables validation

Simulation					Experimentation					Relative error				
Line Current	Motor Current	Line Voltage	Motor Voltage	Freq.	Line Current	Motor Current	Line Voltage	Motor Voltage	Freq.	Line Current	Motor Current	Line Voltage	Motor Voltage	Freq.
A	A	V	V	Hz	A	A	V	V	Hz	%	%	%	%	%
12.3	10.9	220	244	60	11.2	9.9	222	246	59.8	9.82	9.8	0.9	0.73	0.33

Note: RMS values at steady state condition

4. CONCLUSION

In this research, the models of some hydraulic, electromechanical, and mechatronic components belonging to the Simscape libraries in Simulink were studied. These models were integrated to form automatic water flow control systems, based on two case studies: with a control valve (case 1) and with a variable speed drive (case 2). In both cases, the goal of maintaining a constant flow in the event of pressure disturbances generated in the system was met. These case studies do not correspond to a specific process or industry, where there may be specific requirements for the performance of the control system. In those scenarios, a suitable control must be selected and the control system must be carefully designed and configured. Case 2 has some advantages over case 1: at low flow rates, it is more energy-efficient and has less impact on current and torque transients due to the acceleration and deceleration ramps configured in the variable speed drive. A disadvantage of case 2 is the production of harmonics on both the motor and grid sides, which can be reduced with the implementation of harmonic filters. Case 2 model was validated through experimentation, obtaining errors of less than 6% for the hydraulic and mechanical variables, and less than 10% for the electrical ones.

REFERENCES

[1]   E. B. Priyanka, K. Krishnamurthy, and C. Maheswari, "Remote monitoring and control of pressure and flow in oil pipelines transport system using PLC based controller," in *2016 Online International Conference on Green Engineering and Technologies (IC-GET)*, Nov. 2016, pp. 1-6, doi: 10.1109/GET.2016.7916754.

[2]   R. Andrade-Cedeno, "Energy management of a pumping station through the use of statistical process control. case study: "la esperanza" aqueduct - pacific refinery (in Spanish: Gestión energética de una estación de bombeo mediante el uso del control estadístico de procesos. estudio de caso: acueducto "la esperanza" - refinería del pacífico)," *Revista Politécnica*, vol. 40, no. 2, pp. 7-18, 2018.

[3]   M. D. Azari, A. P. Rizi, and A. Ashrafzadeh, "Hydraulic design and operation of variable-speed pumps as the water–energy saving strategies in pressurized irrigation systems," *Clean Technologies and Environmental Policy*, vol. 23, no. 5, pp. 1493-1508, 2021, doi: 10.1007/s10098-021-02043-w.

[4]   R. J. Andrade-Cedeno, "Teaching module for controlling water level and flow, by means of SCADA system, PLC and PID algorithm (in Spanish: Módulo didáctico para controlar nivel y caudal de agua, mediante sistema SCADA, PLC y algoritmo PID)," *RIEMAT*, vol. 4, no. 2, pp. 50-62, 2019, doi: 10.33936/riemat.v4i2.2196.

[5]   V. K. A. Shankar, S. Umashankar, S. Paramasivam, and N. Hanigovszki, "A comprehensive review on energy efficiency enhancement initiatives in centrifugal pumping system," *Applied Energy*, vol. 181, pp. 495-513, 2016, doi: 10.1016/j.apenergy.2016.08.070.

[6]   M. Paun, *Control valve handbook*. 5 ed. Marshalltown, USA: Fisher Controls International LLC, 2019.

[7]   L. Gevorkov, A. Rassõlkin, A. Kallaste, and T. Vaimann, "Simulink based model of electric drive for throttle valve in pumping application," in *2018 19th International Scientific Conference on Electric Power Engineering (EPE)*, 2018, pp. 1-4, doi: 10.1109/EPE.2018.8395996.

[8]   S. Vijayalakshmi, C. Anuradha, R. C. Ilambirai, and V. Ganesh, "Real-time monitoring and control of flow rate in transportation pipelines using matlab-based interactive GUI and PID controller," *International Journal of Power Electronics and Drive System (IJPEDS)*, vol. 11, no. 4, pp. 1767-1774, 2020, doi: 10.11591/ijpeds.v11.i4.pp1767-1774.

[9]   R. J. Andrade-Cedeno and J. A. Perez-Rodriguez, "Analysis of V/f control with SVM in a variable speed drive (in Spanish: Análisis del control V/f con SVM en un accionamiento de velocidad variable)," *Dominios de la Ciencias*, vol. 7, no. 6, pp. 38-62, 2021.

[10] V. K. A. Shankar, S. Umashankar, S. Paramasivam, and H. Norbert, "Real time simulation of variable speed parallel pumping system," *Energy Procedia*, vol. 142, pp. 2102-2108, 2017, doi: 10.1016/j.egypro.2017.12.612.

[11] L. Gevorkov, V. Vodovozov, and Z. Raud, "Simulation study of the pressure control system for a centrifugal pump," in *2016 57th International Scientific Conference on Power and Electrical Engineering of Riga Technical University (RTUCON)*, 2016, pp. 1-5, doi: 10.1109/RTUCON.2016.7763086.

[12] L. Gevorkov, A. Rassõlkin, A. Kallaste, and T. Vaimann, "Simulink based model for flow control of a centrifugal pumping system," in *2018 25th International Workshop on Electric Drives: Optimization in Control of Electric Drives (IWED)*, 2018, pp. 1-4, doi: 10.1109/IWED.2018.8321399.

[13] Y. Wu, X. Guo, G. Li, and C. Lu, "Analysis of shaft power of centrifugal pump under variable speed condition," in *2017 12th IEEE Conference on Industrial Electronics and Applications (ICIEA)*, 2017, pp. 248-252, doi: 10.1109/ICIEA.2017.8282851.

[14] I. J. Karassik, J. P. Messina, P. Cooper, and C. C. Heald, *Pump Handbook*. 3ed. New York, USA: McGraw-Hill, 2001.

[15] B. Kelechava, "Rotodynamic (centrifugal and vertical) pumps - guideline for allowable operating region," *American National Standard Institute (ANSI)*, 2017. [Online]. Available: https://blog.ansi.org/2017/07/ansihi-963-2017-rotodynamic-pumps-aor-bep/

[16] J. Viholainen, "Energy-efficient control strategies for variable speed driven parallel pumping systems based on pump operation point monitoring with frequency converters," M.S. thesis, Institute of Energy Technology, Lappeenranta University of Technology, Lappeenranta, Finlandia, 2014.

[17] MathWorks, "Hydraulic resistive tube," 2022. [Online]. Available: https://la.mathworks.com/help/physmod/simscape/ref/hydraulicresistivetube.html [Accessed Jan. 12, 2022]

[18] MathWorks, "Centrifugal pump with choice of parameterization options,". [Online]. Available: https://la.mathworks.com /help/physmod/hydro/ref/centrifugalpump.html [Accessed Jan. 12, 2022].

[19] MathWorks, "Flow coefficient parameterized valve (TL)," 2022. [Online]. Available: https://la.mathworks.com/help/physmod/hydro/ref/ flowcoefficientparameterizedvalvetl.html [Accessed Jan. 12, 2022].

[20] MathWorks, "DC motor model with electrical and torque characteristics and fault modeling," 2022. [Online]. Available: https://la.math works.com/help/physmod/sps/ref/dcmotor.html [Accessed Jan. 12, 2022].

[21] MathWorks, "Gear box in mechanical systems," 2022. [Online]. Available: https://la.mathworks.com/help/physmod/simscape/ref/gearbox.html [Accessed Jan. 12, 2022].

[22] MathWorks, "Rack and pinion gear coupling translational and rotational motion, with adjustable pinion radius and friction losses,". [Online]. Available: https://la.mathworks.com/help/physmod/sdl/ref/rackpinion.html [Accessed Jan. 12, 2022].

[23] MathWorks, "PWM-controlled DC motor,". [Online]. Available: https://la.mathworks.com/help/physmod/sps/ug/pwm-controlled-dc-motor.html [Accessed Jan. 12, 2022].

[24] L. Jiang, L. Liu, X. Peng, and Z. Xu, "Design and analysis of a fully variable valve actuation system," *Energies*, vol. 13, no. 23, 2020, doi: 10.3390/en13236391.

[25] G. Tosun, O. C. Kivanc, E. Oguz, Y. Mutlu, and O. Ustun, "Design of a position controlled electric actuator used in fluid control valves," in *2016 IEEE International Power Electronics and Motion Control Conference (PEMC)*, 2016, pp. 551-556, doi: 10.1109/EPEPEMC.2016.7752055.

[26] MathWorks, "Model dynamics of three-phase asynchronous machine, also known as induction machine, in SI or pu units,". [Online]. Available: https://la.mathworks.com/help/physmod/sps/powersys/ref/asynchronousmachine.html [Accessed Jan. 12, 2022].

[27] MathWorks, "Implement Clarke and Park transforms for motor control (in Spanish: Implemente transformadas de Clarke y Park para el control de motores),". [Online]. Available: https://la.mathworks.com/solutions/power-electronics-control/clarke-and-park-transforms.html [Accessed Jan. 12, 2022].

[28] MathWorks, "Simulate an AC motor drive,". [Online]. Available: https://la.mathworks.com/help/physmod/sps/powersys/ug/simulating-an-ac-motor-drive.html [Accessed Jan. 12, 2022].

[29] MathWorks, "Implement universal power converter with selectable topologies and power electronic devices,". [Online]. Avaolable: https://la.mathworks.com/help/physmod/sps/powersys/ref/universalbridge.html [Accessed Jan. 12, 2022].

[30] MathWorks, "Implement space vector PWM VSI induction motor drive,". [Online]. Available: https://la.mathworks.com /help/physmod/sps/powersys/ref/spacevectorpwmvsiinductionmotordrive.html [Accessed Jan. 12, 2022].

[31] S. Ojha and A. K. Pandey, "Close loop V/F control of voltage source inverter using sinusoidal PWM, third harmonic injection PWM and space vector PWM method for induction motor," *International Journal of Power Electronics and Drive System (IJPEDS)*, vol. 7, no.1, pp. 217-224, 2016.

[32] H. Sarhan and R. Issa, "Selection of slip compensation technique in three-phase induction motors drive system," *International Journal of Emerging Technology and Advanced Engineering*, vol. 9, no. 12, pp. 9-15, 2019.

[33] Y. Lozanov, S. Tzvetkova, and A. Petleshkov, "Study of the effectiveness of a variable frequency drive of an induction motor," in *2019 11th Electrical Engineering Faculty Conference (BulEF)*, 2019, pp. 1-6, doi: 10.1109/BulEF48056.2019.9030775.

[34] E. Agamloh, A. Cavagnino, and S. Vaschetto, "Induction machine efficiency at variable frequencies," in *2019 IEEE Energy Conversion Congress and Exposition (ECCE)*, 2019, pp. 1655-1662, doi: 10.1109/ECCE.2019.8912969.

[35] C. Burt, X. Piao, F. Gaudi, B. Busch, and N. F. Taufik, "Electric motor efficiency under variable frequencies and loads," *Journal of Irrigation and Drainage Engineering-ASCE*, vol. 134, pp. 129-136, 2008, doi: 10.1061/(ASCE)0733-9437(2008)134:2(129).

[36] S. Greenwood, "Soft starter benefits in pump control," *World Pumps*, vol. 2015, no. 2, pp. 24-27, 2015, doi: 10.1016/S0262-1762(15)70025-8.

[37] D. Lale, M. Oršulić, and I. Palunko, "Modelling and soft-start control of measurement and transport line," *2020 International Conference on Smart Systems and Technologies (SST)*, 2020, pp. 59-64, doi: 10.1109/SST49455.2020.9264077.

[38] N. Matanov, "Study of the impact of induction motors starting on the supply voltage," *2019 16th Conference on Electrical Machines, Drives and Power Systems (ELMA)*, 2019, pp. 1-5, doi: 10.1109/ELMA.2019.8771585.

[39] M. Habyarimana and D. G. Dorrell, "Methods to reduce the starting current of an induction motor," *2017 IEEE International Conference on Power, Control, Signals and Instrumentation Engineering (ICPCSI)*, 2017, pp. 34-38, doi: 10.1109/ICPCSI.2017.8392319.

[40] E. B. Agamloh, S. Peele, and J. Grappe, "Operation of variable frequency drive motor systems with source voltage unbalance," *2017 Annual Pulp, Paper And Forest Industries Technical Conference (PPFIC)*, 2017, pp. 1-9, doi: 10.1109/PPIC.2017.8003869.

[41] B. Narayanasamy, A. S. Sathyanarayanan, A. Deshpande, and F. Luo, "Impact of cable and motor loads on wide bandgap device switching and reflected wave phenomenon in motor drives*," 2017 IEEE Applied Power Electronics Conference and Exposition (APEC)*, 2017, pp. 931-937, doi: 10.1109/APEC.2017.7930808.

[42] B. Narayanasamy, A. S. Sathyanarayanan, F. Luo, and C. Chen, "Reflected wave phenomenon in SiC motor drives: consequences, boundaries, and mitigation," *IEEE Transactions on Power Electronics,* vol. 35, no. 10, pp. 10629-10642, 2020, doi: 10.1109/TPEL.2020.2975217.

[43] H. G. Beleiu, V. Maier, S. G. Pavel, I. Birou, C. S. Picǎ, and P. C. Dǎrab, "Harmonics consequences on drive systems with induction motor," *Applied Sciences*, vol. 10, no. 4, 2020, doi: 10.3390/app10041528.

[44] J. P. Srividhya, D. Sivakumar, and T. Shanmathi, "A review on causes, effects, and detection techniques of harmonics in the power system," *2016 International Conference on Computation of Power, Energy Information and Commuincation (ICCPEIC)*, 2016, pp. 680-686, doi: 10.1109/ICCPEIC.2016.7557309.

[45] A. Kalair, N. Abas, A. R. Kalair, Z. Saleem, and N. Khan, "Review of harmonic analysis, modeling and mitigation techniques," *Renewable and Sustainable Energy Reviews*, vol. 78, pp. 1152-1187, 2017, doi: 10.1016/j.rser.2017.04.121.

BIOGRAPHIES OF AUTHORS

Rogger José Andrade-Cedeno (iD) (g) (SC) (P) he was born in Chone, Ecuador, in 1985. He received the Bachelor's Degree in Electronics and Control Engineering from the National Polytechnic School in 2010. He received the Master's Degree in Quality Management Systems from the Private Technical University of Loja in 2017, and the Master's Degree in Electrical Engineering (mention: Power Systems) from the Technical University of Manabí in 2022. He is currently an assoiate professor at the Technical and Technological Training Academic Unit, ULEAM. Mr. Andrade has collaborated on different projects and operations related to the oil industry, pumping stations, pipelines and aqueducts, and water distribution systems. His research interests are in energy and power systems, electric machines and drives, automation and control systems. He can be contacted at email: rogger.andrade@uleam.edu.ec.

Jesús Alberto Pérez-Rodríguez ⓘ 🔍 sc Ⓟ he was born in Cagua, Venezuela in 1963. He graduated in Electrical Engineering at the University of Carabobo, Valencia, Venezuela in 1988, and M.Sc. and Ph.D. in Sciences (mention: Instrumentation) at the Central University of Venezuela, Caracas, Venezuela, 2002 respectively. His works were developed in the field of robotics and automation, in addition to works on the teaching of Engineering. He has participated in numerous projects aimed at energy efficiency. He can be contacted at email: jesus.perez@utm.edu.ec.

Carlos David Amaya-Jaramillo ⓘ 🔍 sc Ⓟ full-time professor in the Department of Electricity of the Quevedo State Technical University (UTEQ), Quevedo, Ecuador. He graduated in Electronic and Control Engineering in 2010 at the National Polytechnic School, Quito, Ecuador. He defended his doctorate in the Polytechnic University of Madrid in 2018. He can be contacted at email: camaya@uteq.edu.ec.

Ciaddy Gina Rodríguez-Borges ⓘ 🔍 sc Ⓟ she was born in Puerto Ordaz, Venezuela in 1970. She graduated in Industrial Engineering, Master in Business Management (mention: Industrial Management), from the University of Zulia, Venezuela 1999, and Doctor in Technical Sciences, from the Technological University of Havana, Cuba 2012. She has been a professor at the University of Zulia and is currently a Principal Professor at the Technical University of Manabí in the Department of Industrial Engineering. She has been a worker and researcher for the electricity company in Venezuela. Her research work has addressed issues associated with energy efficiency, the use of hybrid energy systems and in areas related to the teaching of engineering. She can be contacted at email: ciaddy.rodriguez@utm.edu.ec.

Endrickson Ramón Vera-Cedeno ⓘ 🔍 sc Ⓟ He was born in Chone, Ecuador in 1969. He graduated in Electrical Engineering in 2013 at the Eloy Alfaro Secular University of Manabí (ULEAM), and is currently an associate professor in the Academic Unit of Technical and Technological Training of the same institution. He is a specialist in the maintenance of electrical systems. He can be contacted at email: endrickson15@gmail.com.

Luis Santiago Quiroz-Fernándes ⓘ 🔍 sc Ⓟ Civil Engineer, Ph.D. in Technical Sciences, current Rector-elect of the Manabí Technical University, Former Director of the Postgraduate Institute of UTM, specialist in the area of Hydraulic Engineering and outstanding manager of public institutions and as a professor of the Civil Engineering career of the UTM. He can be contacted at email: santiago.quiroz@utm.edu.ec.

Yolanda Eugenia Llosas-Albuerne ⓘ 🔍 sc Ⓟ full-time principal professor in the Department of Electricity of the Technical University of Manabí (UTM), Portoviejo Ecuador. She graduated from the Department of Electrical Engineering in Automatic Control in 1979 at the Universidad de Oriente, Cuba, and defended her doctorate in Technical Sciences in 1992. She can be contacted at email: yolanda.llosas@utm.edu.ec.